The Cryosphere Discuss., 6, 4037–4069, 2012
www.the-cryosphere-discuss.net/6/4037/2012/
doi:10.5194/tcd-6-4037-2012

The Cryosphere Discussions

Numerical mass conservation issues in shallow ice models of mountain glaciers: the use of flux limiters and a benchmark

A. H. Jarosch[1], C. G. Schoof[2], and F. S. Anslow[3]

[1]Centre for Climate and Cryosphere, Institute of Meteorology and Geophysics, University of Innsbruck, Innsbruck, Austria
[2]Department of Earth and Ocean Sciences, University of British Columbia, Vancouver, Canada
[3]Pacific Climate Impacts Consortium, University of Victoria, Victoria, Canada

Received: 27 August 2012 – Accepted: 3 September 2012 – Published: 21 September 2012

Correspondence to: A. H. Jarosch (alexander.jarosch@uibk.ac.at)

Published by Copernicus Publications on behalf of the European Geosciences Union.

Abstract

Numerical simulation of glacier dynamics in mountainous regions using low-order, shallow ice models is desirable for computational efficiency and their capability of including ice dynamics in estimates of mountain glacier wastage worldwide. However, these models present several difficulties when applied to complex topography. One such problem arises where dynamical mass flux over steep topography produces spurious mass at a grid cell flux boundary if upstream cells receive positive mass balance. This paper describes a vertically integrated, shallow ice model using a second order flux limiting spatial discretization scheme that enforces mass conservation. An exact solution to ice flow over a bedrock step is derived for a given mass balance forcing as a benchmark to evaluate the model performance in such a difficult setting. This benchmark should serve as a useful test for modellers interested in simulating glaciers over complex terrain.

1 Introduction

The numerical simulation of earth's glaciers and ice sheets is of growing importance to a thorough understanding of our planet's response to climate change. These ice masses are of special importance to concerns about changing water resources and rising sea levels. Although the vast majority of fresh water capable of causing sea level rise over the long-term lies in the Antarctic and Greenland ice sheets, arguably the glaciers most susceptible to climate change in the near future lie at moderate to high latitudes in mountainous terrain. It has been shown that these glaciers are the largest contributor to contemporary sea level rise and that they will contribute substantially to sea level rise in the coming century (e.g. Radić and Hock, 2011; Marzeion et al., 2012)

This importance of alpine glaciers to sea level rise creates a need to understand their behaviour in coming decades. One approach is to explicitly simulate glaciers at a sub-kilometer resolution over large, ice-covered regions of the globe. Such an approach demands models of ice dynamics capable of simulating mountain glaciers but with numerical complexity that allows the simulation of $O(10^7)$ grid nodes over century-long model periods. High order ice dynamical models are capable of simulating individual glaciers or large icesheets, but presently their computational demands restrict their use over domains with very large numbers of grid nodes. By reducing the complexity of the stresses that are simulated in a dynamical model, greater computational effort can be put into addressing large scale problems at some cost to model accuracy. One such model is the vertically integrated, shallow-ice formulation such as the finite element solution described by Fastook and Chapman (1989). A similar formulation has been used to simulate mountain glacier complexes in the Sierra Nevada, USA during the last deglaciation (Plummer and Phillips, 2003) and glacier advances on the summit of Mauna Kea, Hawaii during the last deglaciation (Anslow et al., 2010).

One major problem with standard numerical solvers for shallow ice models is a tendency not to conserve mass in regions where thin ice is draped over steep bed topography. Many of the spatial discretization schemes developed for ice sheets (Huybrechts and Payne, 1996), where steep bed topography is rarely an issue, will spuriously create mass there. Where surface gradients are large, this mass creation can lead to very large errors in modelled steady states. This paper describes the application of a second order flux limiting spatial scheme to the numerical solution of such a model that ensures mass conservation. Furthermore, we describe a benchmark test case along with an analytical exact solution upon which models can be tested for mass conservations when such situations arise. Confirming that a shallow-ice model can meet the benchmark described here along with the benchmarks for the transient simulation of a growing ice sheet described by Bueler et al. (2005) is strongly recommended prior to conducting simulations of glaciers over rough topography.

2 Standard shallow ice models and numerical methods

In a Cartesian coordinate system with the xy plane oriented horizontally, the basic shallow ice model for isothermal ice satisfying Glen's law (Glen, 1958) can be cast as (Fowler and Larson, 1978; Morland and Johnson, 1980)

$$\frac{\partial s}{\partial t} + \nabla \cdot \boldsymbol{q} = \dot{m}, \qquad \boldsymbol{q} = \frac{2A(\rho g)^n}{n+2} h^{n+2} |\nabla s|^{n-1} \nabla s, \tag{1}$$

where $s(x,y,t)$ is ice surface elevation, $h(x,y,t) = s(x,y,t) - b(x,y)$ is ice thickness, $b(x,y)$ is bed elevation and A and n are the usual constants in Glen's law, while ρ and g are ice density and acceleration due to gravity, respectively, and $\dot{m}$ is surface mass balance. ∇ is the usual two-dimensional gradient operator.

Importantly, Eq. (1) holds only where there is ice, so where $h > 0$, and shallow ice models are intrinsically free boundary models in which parts of the domain may be ice free. A complete formulation of the ice flow problem must therefore incorporate a means of evolving ice-covered and ice-free parts of the domain geometrically. In ice-free parts of the domain, $h = 0$ and $s = b$. Ice will grow if $\dot{m} > 0$, but not otherwise. Taken together, this implies that, when $h = 0$,

$$\frac{\partial s}{\partial t} + \nabla \cdot \boldsymbol{q} \geq \dot{m}, \tag{2}$$

and negative ice thicknesses are never realized, as is required physically. In addition, at the ice margin (the free boundary between regions where $h = 0$ and $h > 0$), mass must be conserved and in addition we expect the surface s to be at least continuous. This implies

$$\boldsymbol{q} \cdot \boldsymbol{n} = 0, \qquad h = 0 \tag{3}$$

at this free boundary, with $\boldsymbol{n}$ normal to the free boundary in the xy-plane. The formulation Eq. (1)–(3) is known mathematically as an obstacle problem (Evans, 1998) which can be used to re-write the problem in so-called weak form as a variational inequality (Calvo et al., 2002; Jouvet et al., 2011; Jouvet and Bueler, 2012). This allows various theoretical advances to be made, mostly in demonstrating the well-posedness of shallow ice problems.

Our aim here is more practical, and addresses directly a few shortcomings in widely used numerical methods for solving shallow ice problems. A frequently used approach is to treat Eq. (1) as a parabolic (i.e. diffusion) problem, writing it in the form

$$\frac{\partial s}{\partial t} - \nabla \cdot (D \nabla s) = \dot{m} \tag{4}$$

where

$$D(h, |\nabla s|) = \frac{2A(\rho g)^n}{n+2} h^{n+2} |\nabla s|^{n-1} \tag{5}$$

is a diffusion coefficient. This underlies the numerical methods first developed in Mahaffy (1976) and described in more detail in Huybrechts and Payne (1996). Roughly, these update ice surface elevation $s^{\mathrm{i}}(x,y) = s(x,y,t_{\mathrm{i}})$ by using a lagged diffusivity $D^{\mathrm{i}} = D(h^{\mathrm{i}}, |\nabla s^{\mathrm{i}}|)$ and solving for an unconstrained updated ice surface elevation $\tilde{s}^{\mathrm{i}+1}$ through

$$\frac{\tilde{s}^{\mathrm{i}+1} - s^{\mathrm{i}}}{\Delta t} - \nabla \cdot (D^{\mathrm{i}} \nabla \tilde{s}^{\mathrm{i}+1}) = \dot{m}^{\mathrm{i}+1}, \tag{6}$$

where $\Delta t = t^{\mathrm{i}+1} - t^{\mathrm{i}}$. The actual ice thickness is then updated by truncating this solution anywhere the unconstrained ice surface elevation corresponds to negative ice thickness, so

$$s^{\mathrm{i}+1} = \max(\tilde{s}^{\mathrm{i}+1}, b). \tag{7}$$

TCD
6, 4037–4069, 2012

A slightly more self-consistent approach to the inequaltiy constraints governing Eq. (1) and Eq. (3) would be to apply Eq. (6) only where $\tilde{s}^{i+1} > b$, and to demand instead that

$$\frac{\tilde{s}^{i+1} - s^{i}}{\Delta t} - \nabla \cdot (D^{i} \nabla \tilde{s}^{i+1}) \geq \dot{m}^{i+1}, \tag{8}$$

where $\tilde{s}^{i+1} = 0$, while not allowing negative $\tilde{s}^{i+1}$ at all. This is mathematically equivalent of finding the updated ice thickness by minimizing the functional

$$J(\tilde{s}) = \int_{\Omega} \frac{\left(\tilde{s} - s^{i}\right)^{2}}{2\Delta t} + D^{i} |\nabla \tilde{s}|^{2} \mathrm{d}\Omega, \tag{9}$$

subject to $\tilde{s} \geq b$, where Ω is the entire domain (i.e. the union of ice-covered and ice free regions). In other words, $s^{i+1} = \arg\min_{\tilde{s} \geq b} J(\tilde{s})$, and this can be solved numerically using projected successive over-relaxation (PSOR) methods (Glowinski, 1984) that are similar to solving Eq. (6) with the projection step Eq. (7).

Importantly, however, the continuum formulation of Eq. (6)–(7) as well as of Eq. (9) is misleading: $D^{i} = 0$ anywhere the ice thickness h^{i} is zero, suggesting that ice flow alone should not be able to expand the ice covered area, when clearly this should be possible. In the methods described above, a spatial discretization must be applied first, and the nature of this spatial discretization is crucial.

In particular, spatial discretization schemes designed for diffusion equations of the form of Eq. (4) with bounded difffusivities D may spuriously generate negative ice thicknesses. In fact, such methods may not be appropriate at all in settings where bed topography is steep. The easiest way to understand this is to re-write Eq. (1) as a conservation law for ice thickness $h = s - b$,

$$\frac{\partial h}{\partial t} - \nabla \cdot \left[\frac{2A(\rho g)^{n}}{n+2} h^{n+2} |\nabla (b+h)|^{n-1} \nabla (b+h) \right] = \dot{m} \qquad \text{where } h > 0, \tag{10}$$

Discussion Paper | Discussion Paper | Discussion Paper | Discussion Paper |

TCD

6, 4037–4069, 2012

Mountain glacier model benchmark

A. H. Jarosch et al.

with an analogous inequality to Eq. (2) holding where $h = 0$. In steep terrain, the gradient term $\nabla(b+h)$ may now be dominated by bed slope ∇b, leading approximately to the hyperbolic problem (see also Fowler and Larson, 1978)

$$\frac{\partial h}{\partial t} - \nabla \cdot \left[\frac{2A(\rho g)^n}{n+2} h^{n+2} |\nabla b|^{n-1} \nabla b \right] = \dot{m}. \tag{11}$$

In the absence of a surface mass balance term (i.e. when $\dot{m} = 0$), this hyperbolic equation in its continuum form preserves positivity, i.e. given non-negative initial conditions on h, negative h will never be generated. Spatial discretizations appropriate for hyperbolic equations will maintain this property. However, discretizations designed for parabolic problems, including the symmetric centered difference schemes described in, e.g. Huybrechts and Payne (1996), may not preserve positivity for h, and can therefore spuriously generate negative ice thicknesses. The projection step Eq. (7) of course will then set ice thickness back to zero where this occurs. However, in the process, this causes the numerical scheme to create mass, which can severely affect its results.

Two of the most widely used discretizations in ice sheet models are those referred to as "type I" and "type II" by Huybrechts and Payne (1996), and these are appropriate for the primarily diffusive case of small bed slopes. Essentially, we can view these as finite volume discretizations on a regular mesh, with ice surface elevation piecewise constant on each cell. The location of cell centers are (x_k, y_l) on a grid with uniform spacing such that $\Delta x = x_{k+1} - x_k$ and $\Delta y = y_{l+1} - y_l$. We label the cells by indices (k,l) and denote the normal component of flux on cell boundaries such that the y-component of flux on the cell edge between cells (k,l) and $(k,l+1)$ is $q^y_{k,l+\frac{1}{2}}$ and the x-component of flux on the cell edge between cells (k,l) and $(k+1,l)$ is $q^x_{k+\frac{1}{2},l}$ (Fig. 1).

TCD
6, 4037–4069, 2012

The type I and II schemes both relate these fluxes to differences in surface elevation through

$$q^{y,\mathrm{i}+1}_{k,l+\frac{1}{2}} = -D^{\mathrm{i}}_{k,l+\frac{1}{2}} \frac{\tilde{s}^{\mathrm{i}+1}_{k,l+1} - \tilde{s}^{\mathrm{i}+1}_{k,l}}{\Delta y} \tag{12}$$

$$q^{x,\mathrm{i}+1}_{k+\frac{1}{2},l} = -D^{\mathrm{i}}_{k+\frac{1}{2},l} \frac{\tilde{s}^{\mathrm{i}+1}_{k+1,l} - \tilde{s}^{\mathrm{i}+1}_{k,l}}{\Delta x} \tag{13}$$

where $D^{\mathrm{i}}_{k,l+\frac{1}{2}}$ and $D^{\mathrm{i}}_{k+\frac{1}{2},l}$ are the diffusivities evaluated on the cell boundaries. The fully discretized version of Eq. (4) is then

$$\frac{\tilde{s}^{\mathrm{i}+1}_{k,l} - s^{\mathrm{i}}_{k,l}}{\Delta t} + \frac{q^{x,\mathrm{i}+1}_{k+\frac{1}{2},l} - q^{x,\mathrm{i}+1}_{k-\frac{1}{2},l}}{\Delta x} + \frac{q^{y,\mathrm{i}+1}_{k,l+\frac{1}{2}} - q^{y,\mathrm{i}+1}_{k,l-\frac{1}{2}}}{\Delta y} = \dot{m}^{\mathrm{i}}_{k,l}, \tag{14}$$

and the projection step Eq. (7) is applied cell-wise.

Huybrechts and Payne's type I and II schemes only differ in how they handle the diffusivities $D^{\mathrm{i}}_{k,l+\frac{1}{2}}$ and $D^{\mathrm{i}}_{k+\frac{1}{2},l}$, with type I using an averaged ice thickness at the cell boundary,

$$D^{\mathrm{i}}_{k+\frac{1}{2},l} = \frac{2A(\rho g)^n}{n+2} \left(\frac{h^{\mathrm{i}}_{k,l} - h^{\mathrm{i}}_{k+1,l}}{2} \right)^{n+2} \left[\left(\frac{s^{\mathrm{i}}_{k,l+1} - s^{\mathrm{i}}_{k,l-1} + s^{\mathrm{i}}_{k+1,l+1} - s^{\mathrm{i}}_{k+1,l-1}}{4\Delta y} \right)^2 + \left(\frac{s^{\mathrm{i}}_{k+1,l} - s^{\mathrm{i}}_{k,l}}{\Delta x} \right)^2 \right]^{\frac{n-1}{2}}, \tag{15}$$

and type II using an average over the factor h^{n+2} that appears in the definition of D,

$$D^{\mathrm{i}}_{k+\frac{1}{2},l} = \frac{2A(\rho g)^n}{n+2}\left(\frac{{h^{\mathrm{i}}_{k,l}}^{n+2} - {h^{\mathrm{i}}_{k+1,l}}^{n+2}}{2}\right)$$
$$\left[\left(\frac{s^{\mathrm{i}}_{k,l+1} - s^{\mathrm{i}}_{k,l-1} + s^{\mathrm{i}}_{k+1,l+1} - s^{\mathrm{i}}_{k+1,l-1}}{4\Delta y}\right)^2 + \left(\frac{s^{\mathrm{i}}_{k+1,l} - s^{\mathrm{i}}_{k,l}}{\Delta x}\right)^2\right]^{\frac{n-1}{2}}. \tag{16}$$

With these discretizations, Mahaffy's projection scheme has performed well in many ice sheet models, and in particular, has reproduced a number of known analytical solutions outlined in Bueler et al. (2005, 2007). However, these analytical benchmarks all refer to the case of a flat bed, for which we have $h = s$. Our aim here is to explore a number of complications that arise precisely when this is not the case. That is, we wish to study complications that are typically associated with bed undulations, and which become particularly relevant for modelling mountain glaciation.

3 Mass conservation problems in Mahaffy's scheme

One simple yet problematic case is the one of a mountain glacier sitting in a u-shaped valley. Mahaffy's scheme with a type I or type II diffusivity can generate a spurious mass flux out of the bare rock sidewall of a u-shaped valley into a glacier in the bottom of that valley. Here, we have a cell in which $h^{\mathrm{i}}_{k,l} = s^{\mathrm{i}}_{k,l} - b_{k,l} = 0$ adjacent to a cell in which $h^{\mathrm{i}}_{k+1,l} > 0$ and yet we also have $s^{\mathrm{i}}_{k,l} > s^{\mathrm{i}}_{k+1,l}$, as displayed in Fig. 2a[1]. That is, the ice-free cell has a higher surface elevation than the ice-covered cell. Consequently we

[1]Subsequently we focus on mass conservation problems along the x-axis, but they can equally be generated in three dimensions.

expect that $q^{x}_{k+\frac{1}{2},l}$ and either type I or type II scheme above predict ice flowing from the ice-free into the ice-covered cell. If ice does flow out of the ice-free cell, then the time stepping scheme (Eq. 14) will predict a negative ice thickness for the respective cell after a single time step. The post-processing step (Eq. 7) then sets the actual surface elevation $s^{i+1}_{k,l}$ back to the bed elevation $b_{k,l}$. In terms of mass conservation, we have just extracted mass from the ice-free cell (k,l) and transferred it to the ice-covered cell $(k+1,l)$. In the post processing step (Eq. 7), we have added that mass back into the cell (k,l) in a bid to avoid unphysical negative ice thickness. Formulated this way, Mahaffy's scheme therefore creates mass.

This mass conservation issue was previously recognized by Plummer and Phillips (2003), who proposed a slightly modified scheme that prevents such a mass violation. In particular, Plummer and Phillips (2003) set $D^{i}_{k+\frac{1}{2},l}$ to either the type I or type II values suggested above except at cell boundaries that correspond to a glacier-rock wall boundary. These can be recognized as boundaries with indices $(k+\frac{1}{2},l)$ for which we have

$$(s^{i}_{k,l}-s^{i}_{k+1,l})(h^{i}_{k,l}-h^{i}_{k,l})<0 \quad \text{and} \quad h^{i}_{k,l}h^{i}_{k+1,l}=0. \tag{17}$$

The first of these statements says that ice thickness is greater in the cell that is at a lower elevation, while the second statement says that one of the cells has zero ice thickness (which must therefore be the one with the greater surface elevation). For these cell boundaries, Plummer and Phillips (2003) set $D^{i}_{k+\frac{1}{2},l}=0$ and they also apply an analogous scheme for $D^{i}_{k,l+\frac{1}{2}}$ at cell boundaries parallel to the y-axis.

There is however another possible complication that is not captured by this adjustment of diffusivities. This can occur when a relatively thin glacier flows over a steep bedrock step, as in an icefall. Figure 2b shows the situation we have in mind. Here we can generate a significant ice flux out of the upstream grid cell (k,l) at the top of the ice fall, simply because of the large surface slope between the upstream cell (k,l)

TCD
6, 4037–4069, 2012
Mountain glacier model benchmark
A. H. Jarosch et al.

and the downstream cell $(k+1,l)$.This large flux can then lead to more ice flowing out of the grid cell (k,l) in a single time step from t_{i} to $t_{\mathrm{i}+1}$ than was present at time t_{i}. The updated ice thickness value $\tilde{s}_{k,l}^{\mathrm{i}+1} - b_{k,l}$ becomes negative after a single time step and the projection step (Eq. 7) sets it $s_{k,l}^{\mathrm{i}+1}$ back to zero. A small amount of ice mass is created in the process. At time $t_{\mathrm{i}+2}$, the upstream cell is likely to acquire a non-zero ice thickness $s_{k,l}^{\mathrm{i}+2}$ again as ice can flow into it from above with $q_{k-\frac{1}{2},l}^{x,\mathrm{i}+2} > 0$, which is possible in Plummer and Philips' scheme, but cannot flow out since Eq. (17) is satisfied at the downstream boundary during this time step. After time $t_{\mathrm{i}+2}$, we can therefore return to the same situation as time t_{i}, with a thin ice cover in cell (k,l) and a steep surface slope into cell $(k+1,l)$. Mass can therefore be created on alternating time steps, causing the resulting error to grow over time.

The main reason why the type I and type II schemes above are able to create mass in this way is that they do not limit the flux across a cell boundary as the ice thickness in the upstream cell goes to zero. Consider a vanishingly small ice thickness in cell (k,l) whose bed elevation is greater than the surface elevation in the next cell downstream, $b_{k,l} > s_{k+1,l}^{\mathrm{i}}$. With a type I scheme, the flux across the $k+\frac{1}{2},l$ cell boundary is then still

$$q_{k+\frac{1}{2},l}^{x,\mathrm{i}+1} = \frac{2A(\rho g)^n}{n+2}\left(\frac{h_{k+1,l}^{\mathrm{i}}}{2}\right)^{n+2}\left|\frac{s_{k+1,l}^{\mathrm{i}+1} - b_{k,l}^{\mathrm{i}}}{\Delta x}\right|^{n-1}\frac{b_{k,l}^{\mathrm{i}} - s_{k+1,l}^{\mathrm{i}}}{\Delta x}, \tag{18}$$

which does not go to zero as $h_{k,l}$ does, and a finite amount of mass can therefore still be extracted from a cell with vanishingly small mass content. This occurs because the diffusivity on the cell boundary is dominated by the non-zero ice thickness in the downstream cell $(k+\frac{1}{2},l)$. An analogous observation applies to type II schemes.

Below, we will illustrate this shortcoming of type I and type II discretizations further by showing that they fail to reproduce certain analytic steady state solutions to the shallow ice equations. Before we do so, we propose an alternative scheme for computing diffusivities that alleviates the mass conservation issue described above.

TCD
6, 4037–4069, 2012

4 A mass-conserving scheme

The difficulties of conserving mass with both, type I and type II schemes, are all rooted in the computation of the diffusivities $D^{i}_{k+\frac{1}{2},l}$ and $D^{i}_{k,l+\frac{1}{2}}$. These numerical artifacts stem from the evaluation of the ice thickness term h^{n+2} in the definition of diffusivity (Eq. 5). In both schemes, h on the $(k+\frac{1}{2},l)$ cell boundary is evaluated numerically as an average over the ice thicknesses in the adjacent cells. Consequently, the diffusivity on the cell boundary does not go to zero when the ice thickness in just one of these cells goes to zero.

When there is an advancing ice margin, it is important that the diffusivity should not go to zero at a cell boundary adjoining the ice free cell. Otherwise ice could never flow from an ice-covered cell into an ice free cell, and the ice margin could never advance due to flow. However, we need to avoid the reverse situation in which too much ice flows from a barely ice-covered cell into another cell with lower surface elevation.

To do this, a flux limiting scheme is required and one can adapt a second order Monotone Upstream-centered Schemes for Conservation Laws (MUSCL, e.g. van Leer, 1979; Gottlieb and Shu, 1998) for the ice flux discretization, which is total variation diminishing. A distinct feature of MUSCL schemes is the separation of flux at the cell boundary $(k+\frac{1}{2},l)$ into two components, the $(k+\frac{1}{2}^{+},l)$ and $(k+\frac{1}{2}^{-},l)$ term, which we define below for our application along with the two components for the $(k-\frac{1}{2},l)$ cell boundary. Ice thickness h at the cell boundary is once again the dominant term in the flux discretization, so we can define

$$h^{\mathrm{i}}_{k+\frac{1}{2}^-,l} = h^{\mathrm{i}}_{k,l} + \frac{1}{2}\phi(r_{k,l})(h^{\mathrm{i}}_{k+1,l} - h^{\mathrm{i}}_{k,l}) \tag{19}$$

$$h^{\mathrm{i}}_{k+\frac{1}{2}^+,l} = h^{\mathrm{i}}_{k+1,l} - \frac{1}{2}\phi(r_{k+1,l})(h^{\mathrm{i}}_{k+2,l} - h^{\mathrm{i}}_{k+1,l}) \tag{20}$$

$$h^{\mathrm{i}}_{k-\frac{1}{2}^-,l} = h^{\mathrm{i}}_{k,l} + \frac{1}{2}\phi(r_{k-1,l})(h^{\mathrm{i}}_{k,l} - h^{\mathrm{i}}_{k-1,l}) \tag{21}$$

$$h^{\mathrm{i}}_{k-\frac{1}{2}^+,l} = h^{\mathrm{i}}_{k+1,l} - \frac{1}{2}\phi(r_{k,l})(h^{\mathrm{i}}_{k+1,l} - h^{\mathrm{i}}_{k,l}) \tag{22}$$

with

$$r_{k,l} = \frac{h^{\mathrm{i}}_{k,l} - h^{\mathrm{i}}_{k-1,l}}{h^{\mathrm{i}}_{k+1,l} - h^{\mathrm{i}}_{k,l}} \tag{23}$$

the ratio of downstream to upstream ice thickness change and $\phi(r_{k,l})$ being the flux limiting function. We investigate the usability of two flux limiters in our study, the minmod limiter $\phi_{\mathrm{mm}}(r)$ and superbee limiter $\phi_{\mathrm{sb}}(r)$ (Roe, 1986):

$$\phi_{\mathrm{mm}}(r) = \max[0, \min(1, \mathrm{r})] \tag{24}$$

$$\phi_{\mathrm{sb}}(r) = \max[0, \min(2\mathrm{r}, 1), \min(\mathrm{r}, 2)]. \tag{25}$$

Using the ice thickness estimates from Eq. (20), we can define two flux terms at the cell boundary

$$D^{\mathrm{i}}_{k+\frac{1}{2}^+,l} = \frac{2A(\rho g)^n}{n+2} h^{\mathrm{i}\;\;n+2}_{k+\frac{1}{2}^+,l} \left[\left(\frac{s^{\mathrm{i}}_{k,l+1} - s^{\mathrm{i}}_{k,l-1} + s^{\mathrm{i}}_{k+1,l+1} - s^{\mathrm{i}}_{k+1,l-1}}{4\Delta y}\right)^2 + \left(\frac{s^{\mathrm{i}}_{k+1,l} - s^{\mathrm{i}}_{k,l}}{\Delta x}\right)^2\right]^{\frac{n-1}{2}} \tag{26}$$

TCD
6, 4037–4069, 2012

and $D^{\mathrm{i}}_{k+\frac{1}{2}^-,l}$ by using Eq. (19) instead of Eq. (20). To limit the flux at the cell boundary, one defines a minimum and maximum diffusivity such that

$$D^{\mathrm{i}}_{k+\frac{1}{2},l,\min} = \min(D^{\mathrm{i}}_{k+\frac{1}{2}^-,l}, D^{\mathrm{i}}_{k+\frac{1}{2}^+,l}) \tag{27}$$

$$D^{\mathrm{i}}_{k+\frac{1}{2},l,\max} = \max(D^{\mathrm{i}}_{k+\frac{1}{2}^-,l}, D^{\mathrm{i}}_{k+\frac{1}{2}^+,l}) \tag{28}$$

and constructs a diffusivity for the $(k+\frac{1}{2}, l)$ cell boundary as

$$D^{\mathrm{i}}_{k+\frac{1}{2},l} = \begin{cases} D^{\mathrm{i}}_{k+\frac{1}{2},l,\min} & \text{if } s^{\mathrm{i}}_{k+1,l} \le s^{\mathrm{i}}_{k,l} \text{ and } h^{\mathrm{i}}_{k+\frac{1}{2}^-,l} \le h^{\mathrm{i}}_{k+\frac{1}{2}^+,l}, \\ D^{\mathrm{i}}_{k+\frac{1}{2},l,\max} & \text{if } s^{\mathrm{i}}_{k+1,l} \le s^{\mathrm{i}}_{k,l} \text{ and } h^{\mathrm{i}}_{k+\frac{1}{2}^-,l} > h^{\mathrm{i}}_{k+\frac{1}{2}^+,l}, \\ D^{\mathrm{i}}_{k+\frac{1}{2},l,\max} & \text{if } s^{\mathrm{i}}_{k+1,l} > s^{\mathrm{i}}_{k,l} \text{ and } h^{\mathrm{i}}_{k+\frac{1}{2}^-,l} \le h^{\mathrm{i}}_{k+\frac{1}{2}^+,l}, \\ D^{\mathrm{i}}_{k+\frac{1}{2},l,\min} & \text{if } s^{\mathrm{i}}_{k+1,l} > s^{\mathrm{i}}_{k,l} \text{ and } h^{\mathrm{i}}_{k+\frac{1}{2}^-,l} > h^{\mathrm{i}}_{k+\frac{1}{2}^+,l}, \end{cases} \tag{29}$$

The diffusivities $D^{\mathrm{i}}_{k-\frac{1}{2},l}$, $D^{\mathrm{i}}_{k,l+\frac{1}{2}}$, and $D^{\mathrm{i}}_{k,l-\frac{1}{2}}$ can be constructed in a similar manner. Note that the local surface slopes are used to identify the upstream direction, which is needed in a MUSCL scheme to assign the right limited flux terms. We recall that our initial equation was

$$\frac{\partial s}{\partial t} + \nabla \cdot \boldsymbol{q} = \dot{m}, \tag{30}$$

which can be discretized in time, as an alternative to Eq. (6), explicitly using a forward Euler scheme

$$\frac{\tilde{s}^{\mathrm{i}+1} - s^{\mathrm{i}}}{\Delta t} - \nabla \cdot (D^{\mathrm{i}} \nabla s^{\mathrm{i}}) = \dot{m}^{\mathrm{i}}. \tag{31}$$

All that is left to do is to define the gradient of the flux in its fully discretized form:

$$\nabla \cdot (D^{\mathrm{i}} \nabla s^{\mathrm{i}}) = \frac{D^{\mathrm{i}}_{k+\frac{1}{2},l} \frac{s^{\mathrm{i}}_{k+1,l} - s^{\mathrm{i}}_{k,l}}{\Delta y} - D^{\mathrm{i}}_{k-\frac{1}{2},l} \frac{s^{\mathrm{i}}_{k,l} - s^{\mathrm{i}}_{k-1,l}}{\Delta y}}{\Delta y} + \frac{D^{\mathrm{i}}_{k,l+\frac{1}{2}} \frac{s^{\mathrm{i}}_{k,l+1} - s^{\mathrm{i}}_{k,l}}{\Delta x} - D^{\mathrm{i}}_{k,l-\frac{1}{2}} \frac{s^{\mathrm{i}}_{k,l} - s^{\mathrm{i}}_{k,l-1}}{\Delta x}}{\Delta x}. \tag{32}$$

The value for the time step Δt used is crucial in this forward scheme to provide numerically stable solutions. A stability condition can be used to automatically calculate a suitable value as

$$\Delta t = c_{\mathrm{stab}} \frac{\min(\Delta x^2, \Delta y^2)}{\max(D^{\mathrm{i}}_{k+\frac{1}{2},l}, D^{\mathrm{i}}_{k-\frac{1}{2},l}, D^{\mathrm{i}}_{k,l+\frac{1}{2}}, D^{\mathrm{i}}_{k,l-\frac{1}{2}})}. \tag{33}$$

Hindmarsh (2001) analysed time stepping stability criteria and reports for explicit time stepping schemes $c_{\mathrm{stab}} < \frac{1}{2n}$ for one dimensional and $c_{\mathrm{stab}} < \frac{1}{2(n+1)}$ for two dimensional configurations. In case of $n = 3$ this leads to $c_{\mathrm{stab}} < 1.66\dot{6}$ and $c_{\mathrm{stab}} < 1.125$, respectively.

5 One-dimensional steady states

A good way to test a shallow ice code is to compare results with analytically computable solutions (Bueler et al., 2005, 2007). Below we present such a steady-state solution which includes bed topography and a prescribed accumulation rate which is a function of position only. We construct a family of steady state profiles and test how accurately the numerical shallow ice algorithms described above are able to reproduce them.

TCD
6, 4037–4069, 2012

In one dimension with the assumption of steady state, the shallow ice model (Eq. 1) can be written in the form

$$q_x = \dot{m}, \tag{34}$$

where the subscript "x" denotes an ordinary derivative, and

$$q = -\frac{2A(\rho g)^n}{n+2} h^{n+2} |s_x|^{n-1} s_x. \tag{35}$$

To simplify matters, we assume that accumulation rate a depends only on position x and is such that there is a single ice-occupied region occupying the interval $0 < x < x_\mathrm{m}$. Here x_m is the margin position, which must be determined as part of the solution. At $x = x_\mathrm{m}$,

$$h|_{x=x_\mathrm{m}} = 0 \quad q|_{x=x_\mathrm{m}} = 0, \tag{36}$$

and we have

$$h > 0 \quad \text{for } 0 < x < x_s. \tag{37}$$

In addition, we assume that there is no inflow of ice at the fixed upstream boundary $x = 0$. In that case, ice flux q can be found explicitly as a function of position for any $x < x_\mathrm{m}$:

$$q = \int_0^x \dot{m}(x')dx'. \tag{38}$$

To simplify our notation, we write $Q(x) = \int_0^x \dot{m}(x')dx'$. Given $\dot{m}(x)$, $Q(x)$ is then a known function of position. The unknown margin position is then determined implicitly by the second condition in Eq. (36),

$$Q(x_\mathrm{m}) = 0. \tag{39}$$

Given x_m, ice thickness h must then be found as a function of position through solving the differential equation $q = Q(x)$, or

$$-\frac{2A(\rho g)^n}{n+2} h^{n+2} |s_x|^{n-1} s_x = Q(x) \tag{40}$$

subject to the first condition in Eq. (36), $h(x_m) = 0$.

There are no general methods for solving Eq. (40) analytically. To get around this, we restrict our choice of bed topography to generate a tractable problem. Our objective is to develop a test for numerical shallow ice codes that incorporate bed topography. Consequently, we do not wish to put $b \equiv 0$. On the other hand, Eq. (40) is easiest to deal with for a flat bed, in which case $s_x = h_x$. To make use of this, we consider a bed for which b is a step function,

$$b(x) = \begin{cases} b_0 & x < x_s, \\ 0 & x > x_s, \end{cases} \tag{41}$$

where b_0 and x_s are constants, and we assume that $0 < x_s < x_m$.

In the interval $0 < x < x_s$ and $x_s < x < x_m$, this allows us to write Eq. (40) as

$$-\frac{2A(\rho g)^n}{n+2} h^{n+2} |h_x|^{n-1} h_x = Q(x), \tag{42}$$

which we can re-write as

$$h^{\frac{n+2}{n}} h_x = -\left[\frac{(n+2)}{2A(\rho g)^n}\right]^{\frac{1}{n}} |Q(x)|^{\frac{1}{n}-1} Q(x). \tag{43}$$

Integrating using the boundary condition $h(x_m) = 0$, and subsequently solving for h, we get

$$h(x) = \left[\frac{(2n+2)(n+2)^{\frac{1}{n}}}{4A^{\frac{1}{n}}\rho g} \int_x^{x_m} |Q(x')|^{\frac{1}{n}-1} Q(x') dx'\right]^{\frac{2}{2n+2}}. \tag{44}$$

TCD
6, 4037–4069, 2012

in the interval $x_s < x < x_\mathrm{m}$.

At the bedrock step at $x = x_s$, we can therefore define an ice thickness just downstream of the step as

$$h_{s+} = \lim_{x \to x_s^+} h(x) = \left[\frac{(2n+2)(n+2)^{\frac{1}{n}}}{4A^{\frac{1}{n}}\rho g} \int_x^{x_\mathrm{m}} |Q(x')|^{\frac{1}{n}-1} Q(x') dx' \right]^{\frac{2}{2n+2}}. \tag{45}$$

In order to extend the solution to $x < x_s$, we can then integrate Eq. (43) backwards from $x = x_s$:

$$h(x)^{\frac{2n+2}{n}} = h_{s-}^{\frac{2n+2}{n}} + \frac{(2n+2)(n+2)^{\frac{1}{n}}}{4A^{\frac{1}{n}}\rho g} \int_x^{x_\mathrm{m}} |Q(x')|^{\frac{1}{n}-1} Q(x') dx', \tag{46}$$

where $h_{s-} = \lim_{x \to x_s^-} h(x)$. To close this solution, it remains to determine the ice thickness h_{s-} at the top of the bedrock step.

In general, we expect the surface elevation s to be continuous. But $s = h + b$, so this implies

$$h_{s-} + b_0 = h_{s+} \quad \text{or} \quad h_{s-} = h_{s+} - b_0. \tag{47}$$

This must the be substituted in Eq. (46) with h_{s+} given by Eq. (45).

It is, however, possible that h_{s-} computed in this way is negative. Specifically, this occurs when h_{s+} computed in Eq. (45) is less than b_0. In that case, Eq. (47) cannot hold as h will be negative just upstream of the bedrock step, and will therefore violate the condition given in Eq. (37). A more acceptable solution can instead be obtained in the case that $h_{s+} < b_0$ if we put $h_{s-} = 0$ in Eq. (46).

Allowing for this possibility, the required analytical steady-state solution is given by Eqs. (46) and (44), with h_{s-} determined by

$$h_{s-} = \max(h_{s+} - b_0, 0). \tag{48}$$

This solution, with a discontinuity in surface elevation, may seem an unnatural test for a shallow ice model. However, it can be shown that the solution we have given is in fact the correct limit of a solution with a continuous but steep bedrock step as the width of that bedrock step goes to zero. In numerical simulations with finite grid size, steep steps in bed topography may not be well resolved, and it is desirable to have a numerical scheme that remains robust when this is the case.

Crucial to the mechanism for mass creation described in Eq. (18) was a setting in which bedrock elevation $b_{k,l}$ in the upstream cell (k,l) is greater than ice surface elevation $s_{k+1,l}$ in the downstream cell, and this is precisely the situation realized when there is a sufficiently tall bedrock step $h_{s_-} = 0$ as advocated above. In fact, we show explicitly in Appendix A that there are conditions under which type I and II schemes cannot reproduce such steady states.

6 A specific, explicit solution for a bedrock step

The solutions in Eqs. (44) and (46) are still given in terms of the general flux $Q(x) = \int_0^x \dot{m}(x')dx'$. Next, we give a choice $Q(x)$ that allows us to compute h explicitly, and which is such that the corresponding accumulation rate function $\dot{m} = Q'(x)$ is sensible (in particular, which satisfies the obvious requirement that $Q(0) = 0$ and which is such that $\dot{m}$ is negative for $x > x_\mathrm{m}$, so that there is indeed a single ice body in steady state). This is given by

$$Q(x) = \frac{\dot{m}_0}{x_m^{2n-1}} x^n |x_\mathrm{m} - x|^{n-1}(x_\mathrm{m} - x), \tag{49}$$

with a corresponding accumulation rate function

$$\dot{m}(x) = \frac{n\dot{m}_0}{x_m^{2n-1}} x^{n-1} |x_\mathrm{m} - x|^{n-2}(x_\mathrm{m} - x)[|x_\mathrm{m} - x| - x]. \tag{50}$$

Q satisfies $Q(x_\mathrm{m}) = 0$, and x_m can indeed be identified with the steady-state margin position. In addition $\dot{m} < 0$ if $x > x_\mathrm{m}$, so there is no ice outside the margin x_m.

With this choice of a and Q, we have

$$|Q(x')|^{\frac{1}{n}-1}Q(x') = \frac{\dot{m}_0^{\frac{1}{n}}}{x_\mathrm{m}^{\frac{2n-1}{n}}}x(x_\mathrm{m}-x), \tag{51}$$

and hence the ice surface profile in Eqs. (44) and (46) can be computed as

$$h(x) = \left[\frac{(2n+2)(n+2)^{\frac{1}{n}}\dot{m}_0^{\frac{1}{n}}}{24A^{\frac{1}{n}}\rho g x_\mathrm{m}^{\frac{2n-1}{n}}}(x_\mathrm{m}+2x)(x_\mathrm{m}-x)^2\right]^{\frac{2}{2n+2}} \tag{52}$$

for $x_s < x < x_\mathrm{m}$, and

$$h(x) = \left[h_{s-}^{\frac{2n+2}{n}} - h_{s+}^{\frac{2n+2}{n}} + \frac{(2n+2)(n+2)^{\frac{1}{n}}\dot{m}_0^{\frac{1}{n}}}{24A^{\frac{1}{n}}\rho g x_\mathrm{m}^{\frac{2n-1}{n}}}(x_\mathrm{m}+2x)(x_\mathrm{m}-x)^2\right]^{\frac{2}{2n+2}} \tag{53}$$

for $0 < x < x_s$. Here h_{s+} and h_{s-} are given through the calculations

$$h_{s+} = \left[\frac{(2n+2)(n+2)^{\frac{1}{n}}\dot{m}_0^{\frac{1}{n}}}{24A^{\frac{1}{n}}\rho g}(x_\mathrm{m}+2x)(x_\mathrm{m}-x)^2\right]^{\frac{2}{2n+2}} \tag{54}$$

$$h_{s-} = \max(h_{s+} - b_0, 0). \tag{55}$$

TCD
6, 4037–4069, 2012

7 Numerical benchmark experiments

7.1 Cliff benchmark

To demonstrate the performance of our newly introduced scheme and to showcase our explicit solution as a benchmark for numerical ice flow schemes in mountainous regions, we numerically implement Eqs. (13) and (14)[2]. In one case, we use the diffusivity from Eq. (15) and refer to results from this setup as type I results. In the other case, we compute results by using the diffusivity from Eq. (26) along with the superbee flux limiter, Eq. (25), which we label "MUSCL superbee". Using the minmod flux limiter, Eq. (24), gives slightly different results, which we will discuss below. For temporal evolution, we solve Eq. (31) with an adequate stability condition as mentioned earlier.

First let us define a set of parameters for the explicit solution (Eqs. 52 and 53). We use $x_{\mathrm{m}} = 20\,000\,\mathrm{m}$, $x_s = 7000\,\mathrm{m}$, $b_0 = 500\,\mathrm{m}$, $\dot{m}_0 = 2\,\mathrm{m\,yr^{-1}}$, $A = 1 \times 10^{-16}\,\mathrm{yr^{-1}\,Pa^{-3}}$, $n = 3$, $\rho = 910\,\mathrm{kg\,m^{-3}}$, and $g = 9.81\,\mathrm{m\,s^{-2}}$ as well as a spatial resolution of $\Delta x = 200\,\mathrm{m}$. The time stepping stability parameter in Eq. (33) is $c_{\mathrm{stab}} = 0.165$.

Results for the type I scheme and MUSCL superbee scheme are displayed in Fig. 3 in comparison with a result computed with Eqs. (52) and (53). We plot numerical results in 1000 yr intervals for a 50 000 yr evolution of the models. The MUSCL superbee scheme (blue lines in Fig. 3) converges towards the steady-state solution (magenta line in Fig. 3), whereas the classical type I scheme fails to do so and creates a large amount of spurious mass.

We compare volume estimates between the model outputs and the explicit solution. Integrating the steady-state solution results in a target two dimensional volume of $4.443984 \times 10^6\,\mathrm{m^2}$. After 50 000 yr of evolution, the "MUSCL superbee" scheme ends with a volume of $4.399017 \times 10^6\,\mathrm{m^2}$, or a relative error of $-1.012\,\%$. The classical type I scheme leads to a volume of $10.93219 \times 10^6\,\mathrm{m^2}$, or a relative error of $146.0\,\%$. Convergence of the MUSCL scheme with both flux limiters as well as the type I scheme

[2] A Python version of the 1-D code is included in the Supplement.

for different Δx towards the explicit solution is demonstrated in Table 1. Note that the relative error of the type I scheme is increasing with increasing Δx.

The mass conservation problem in Mahaffy's scheme, described in Sect. 3, has been tested with our new scheme as well. We recreate a setup similar to the one displayed in Fig. 2a, with as spatial resolution of $\Delta x = 200$ m and let it evolve of 50 000 yr with $\dot{m} = 0$. The result is displayed in Fig. 4. We monitor the changes in ice volume, which should be zero as $\dot{m} = 0$. After 50 000 yr, the solutions with the MUSCL superbee scheme (blue lines in Fig. 4) as well as the MUSCL minmod scheme (not shown) conserve mass whereas the type I scheme has a relative volume error of −9.5 % in comparison with the intial volume. The earlier decribed modification to the type I scheme, Eq. (17), has not been applied in this comparison, which demonstrated that both of our schemes have no mass conservation difficulties in this test as well. Thus a correction step as described in Eq. (17) is not required when using our schemes.

7.2 Bueler C benchmark

The Bueler C benchmark (Bueler et al., 2005) is an ideal test case to compare finite difference discretization schemes with a time evolving exact solution. In this benchmark, a time evolving mass balance is given to the flow code to grow an ice dome over 15 208 yr, after which the numerical solution is compared to the exact one. We take error in central dome ice thickness, $e_{\text{dome}} = |h_{\text{exact}}(0,0) - h_{\text{num}}(0,0)|$, and maximum ice thickness difference in the whole domain, $e_{\text{max}} = \max(|h_{\text{exact}} - h_{\text{num}}|)$, as our performance measures. Figure 5 displays the decrease in e_{dome} and e_{max} with increasing grid point number, N, for same benchmark setup as displayed in Fig. 7 and 8 in Bueler et al. (2005).

In both cases we demonstrate that the MUSCL scheme can outperform the type I scheme for smaller grid sizes ($N \geq 240$, $\Delta x \leq 6250$ m) if the right flux limiter is chosen, i.e. the superbee limiter (cf. Eq. 25). This is an anticipated result as the MUSCL scheme is second order and thus more accurate than the type I scheme, but it is surprising that

TCD
6, 4037–4069, 2012

an unfortunate choice of flux limiter, i.e. the minmod limiter (cf. Eq. 24), makes the MUSCL scheme perform worse in comparison to the type I scheme.

8 Conclusions

After revisiting a well known mass conservation problem of finite difference models for glacier flow in mountainous regions, we have identified another complication which arises with very steep topography. In that case, several widely-used numerical schemes will extract excess mass from cells with thin ice cover, and subsequently add mass to these cells again to avoid negative ice thicknesses, thereby violating mass conservation.

To overcome both problems, we propose to use a second order flux limiting spatial discretization for the diffusion term in the standard shallow ice equation. In this contribution we have investigated the applicability of a MUSCL scheme with two different flux limiters, the minmod and the superbee.

As a benchmark to evaluate the performance of the MUSCL scheme in comparison to type I and II schemes in such steep topographies, we have derived an exact solution to ice flow over a bedrock step for a given mass balance forcing. Using this newly derived exact solution in combination with the well established exact solutions of Bueler et al. (2005), we find the MUSCL scheme in combination with the superbee flux limiter the best suitable spatial discretization for mountain glacier flow models, which has no difficulties with the above mentioned mass conservation issues.

Our newly developed exact solution for ice flow over a bedrock step adds another case of exact solution based benchmarks to the existing ones (Bueler et al., 2005, 2007), with which numerical ice flow models should be evaluated. If finite difference shallow ice flow models are to be applied in mountainous regions with complex topography, we anticipate that our proposed scheme and benchmark will help significantly to improve and evaluate such models.

TCD
6, 4037–4069, 2012

Appendix A

The failure of type I/type II schemes in computing steady states

With the analytical solutions above in place, we can illustrate further why type I and type II schemes can fail. Consider the discretized steady-state shallow ice equations in one spatial dimension, discretized using a finite volume-type scheme as above. Using only one subscript label to indicate cells numbered along the x-axis, we have

$$\frac{q^x_{k+\frac{1}{2}} - q^x_{k-\frac{1}{2}}}{\Delta x} = \dot{m}_k \tag{A1}$$

for an ice-covered cell, where

$$q^x_{k+\frac{1}{2}} = D_{k+\frac{1}{2}} \frac{s_{k+1} - s_k}{\Delta x}. \tag{A2}$$

Let $q^x_{\frac{1}{2}} = 0$, so the cell boundary to the left of the cell $k = 1$ is a domain boundary with no inflow, corresponding to $x = 0$ in the continuum solutions above. Assuming that cells $1, 2, \ldots, k$ are ice covered, Eq. (A1) then shows that

$$q^x_{k+\frac{1}{2}} = \sum_{j=1}^{k} \dot{m}_j \Delta x, \tag{A3}$$

which is analogous to the statement that $q(x) = \int_0^x \dot{m}(x')\mathrm{d}x'$ in the continuum problem above.

Suppose that there is a single ice mass between $x = 0$ and the margin $x = x_\mathrm{m}$, and that there is no ice for $x > x_\mathrm{m}$. Let the discrete margin position be the cell boundary $k_m + \frac{1}{2}$, so that $h_k > 0$ for $k \le k_m$ but $h_k = 0$ for $k > k_m$, and similarly $q^x_{k+\frac{1}{2}} > 0$ for $k \le k_m$ but $q^x_{k+\frac{1}{2}} = 0$ for $k > k_m$. Equation (A3) of course holds only for $k \le k_m$. It can be shown

TCD
6, 4037–4069, 2012
Mountain glacier model benchmark
A. H. Jarosch et al.

from Mahaffy's projection step that the margin location k_m in steady state is then given by the value of k_m that satisfies both of the following inequalities

$$\sum_{j=1}^{k_m} \dot{m}_j \Delta x > 0 \qquad \text{and} \qquad \sum_{j=1}^{k_m+1} \dot{m}_j \Delta x < 0, \tag{A4}$$

which are equivalent to the statement that $\int_0^{x_\mathrm{m}} \dot{m}(x')\mathrm{d}x' = 0$ in the continuum formulation above; it is easy to show that the margin location defined by these inequalities converges to the continuum solution of $\int_0^{x_\mathrm{m}} \dot{m}(x')\mathrm{d}x'$.

Given a discrete margin location k_m, ice thicknesses h_k for $k \leq k_m$ can then be computed recursively, starting with ice thickness just upstream of the margin at $k = k_m$. For each $k \leq k_m$, we have flux $q^x_{k+\frac{1}{2}}$ explicitly through Eq. (A3). To be definite, consider a type I discretization for diffusivity, though the argument below can also be applied in slightly modified form to a type II discretization. With $s_k = h_k + b_k$, we then have

$$\frac{2A(\rho g)^n}{n+2}\left(\frac{h_k + h_{k+1}}{2}\right)^{n+2}\left|\frac{h_k + b_k - h_{k+1} - b_{k+1}}{\Delta x}\right|\frac{h_k + b_k - h_{k+1} - b_{k+1}}{\Delta x} = \tag{A5}$$

$$q^x_{k+\frac{1}{2}} = \sum_{j=1}^{k} \dot{m}_j \Delta x. \tag{A6}$$

This nonlinear equation must then be solved for h_k given ice thickness h_{k+1} at the next grid cell downstream, as well as the bed elevations b_k and b_{k+1}. This procedure is started with $k = k_m$, for which we have $h_{m+1} = 0$.

Problems arise in this procedure if at some value of k we have $b_k > h_{k+1} + b_{k+1}$. This occurs when surface elevation in the $(k+1)$th cell is lower than bed elevation in the kth cell. If we also demand that $h_k \geq 0$, then one can show that the expression on the left-hand side of Eq. (A5) is bounded below by a quantity q_{min} that depends only on bed geometry and on ice thickness downstream from the current cell,

$$\frac{2A(\rho g)^n}{n+2}\left(\frac{h_k+h_{k+1}}{2}\right)^{n+2}\left|\frac{h_k+b_k-h_{k+1}-b_{k+1}}{\Delta x}\right|\frac{h_k+b_k-h_{k+1}-b_{k+1}}{\Delta x} \geq \tag{A7}$$

$$\frac{2A(\rho g)^n}{n+2}\left(\frac{h_{k+1}}{2}\right)^{n+2}\left|\frac{b_k-h_{k+1}-b_{k+1}}{\Delta x}\right|\frac{b_k-h_{k+1}-b_{k+1}}{\Delta x} = q_{\min}(h_{k+1},b_k,b_{k+1}). \tag{A8}$$

Hence no non-negative solution for h_k can be computed from Eq. (A5) if

$$q^x_{k+\frac{1}{2}} < q_{\min}(h_{k+1},b_k,b_{k+1}).$$

In this situation, the assumption we have made in arriving at Eq. (A5) must break down. In particular, the assumption of a single connected ice mass in which $h_k > 0$ for $k \leq k_m$ must fail for the discrete solution even if it holds for the continuum problem, and the discrete solution will not approximate the continuous solution. Again, this occurs because the flux $q^x_{k+\frac{1}{2}}$ does not go to zero even as the ice thickness h_k in the upstream cell does.

Supplementary material related to this article is available online at: http://www.the-cryosphere-discuss.net/6/4037/2012/tcd-6-4037-2012-supplement.zip.

Acknowledgements. AHJ was supported by the Austrian Science Fund (FWF): P22443-N21. CGS was supported by a Canada Research Chair and NSERC Discovery Grant 357193. This paper is a contribution to the Western Canadian Cryospheric Network, funded by Canada Foundation for Climate and Atmospheric Sciences and a consortium of Canadian universities.

References

Anslow, F. S., Clark, P. U., Kurz, M. D., and Hostetler, S. W.: Geochronology and paleoclimatic implications of the last deglaciation of the Mauna Kea Ice Cap, Hawaii, Earth Planet. Sc. Lett., 297, 234–248, doi:10.1016/j.epsl.2010.06.025, 2010.

Bueler, E., Lingle, C. S., Kallen-Brown, J. A., Covey, D. N., and Bowman, L. N.: Exact solutions and verification of numerical models for isothermal ice sheets, J. Glaciol., 51, 291–306, doi:10.3189/172756505781829449, 2005.

Bueler, E., Brown, J., and Lingle, C.: Exact solutions to the thermomechanically coupled shallow-ice approximation: effective tools for verification, J. Glaciol., 53, 499–516, doi:10.3189/002214307783258396, 2007.

Calvo, N., Díaz, J., Durany, J., Schiavi, E., and Vázquez, C.: On a doubly nonlinear parabolic obstacle problem modelling ice sheet dynamics, SIAM J. Appl. Math., 63, 683–707, 2002.

Evans, L. C.: Partial Differential Equations, Graduate Studies in Mathematics, American Mathematical Society, Providence, 1998.

Fastook, J. L. and Chapman, J. E.: A map-plane finite-element model: three modeling experiments, J. Glaciol., 35, 48–52, doi:10.3189/002214389793701464, 1989.

Fowler, A. C. and Larson, D. A.: On the flow of polythermal glaciers. I. Model and preliminary analysis, Proc. R. Soc. Lond. A, 363, 217–242, doi:10.1098/rspa.1978.0165, 1978.

Glen, J. W.: The flow law of ice. A discussion of the assumptions made in glacier theory, their experimental foundation and consequences, IASH, 47, 171–183, 1958

Glowinski, R.: Numerical Methods for Nonlinear Variational Problems, Springer Series in Computational Physics, Springer-Verlag, New York, 1984.

Gottlieb, S. and Shu, C.-W.: Total variation diminishing Runge-Kutta schemes, Math. Comput., 67, 73–86, doi:10.1090/S0025-5718-98-00913-2, 1998.

Hindmarsh, R.: Notes on basic glaciological computational methods and algorithms, in: Continuum Mechanics and Applications in Geophysics and the Environment, edited by: Straughan, B., Greve, R., Ehrentraut, H., and Wang, Y., Springer Verlag, Berlin Heidelberg, Germany, 222–249, 2001.

Huybrechts, P. and Payne, T.: The EISMINT benchmarks for testing ice-sheet models, Ann. Glaciol., 23, 1–12, 1996.

Jouvet, G. and Bueler, E.: Steady, shallow ice sheets as obstacle problems: well-posedness and finite element approximation, SIAM J. Appl. Math., 72, 1292–1314, doi:10.1137/110856654, 2012.

Jouvet, G., Rappaz, J., Bueler, E., and Blatter, H.: Existence and stability of steady-state solutions of the shallow-ice-sheet equation by an energy-minimization approach, J. Glaciol., 57, 345–354, 2011.

Mahaffy, M. W.: A three-dimensional numerical model of ice sheets: tests on the Barnes Ice Cap, Northwest Territories, J. Geophys. Res., 81, 1059–1066, 1976.

Marzeion, B., Jarosch, A. H., and Hofer, M.: Past and future sea-level change from the surface mass balance of glaciers, The Cryosphere Discuss., 6, 3177–3241, doi:10.5194/tcd-6-3177-2012, 2012.

Morland, L. W. and Johnson, I. R.: Steady motion of ice sheets, J. Glaciol., 25, 229–246, 1980.

Plummer, M. A. and Phillips, F. M.: A 2-D numerical model of snow/ice energy balance and ice flow for paleoclimatic interpretation of glacial geomorphic features, Quaternary Sci. Rev., 22, 1389–1406, doi:10.1016/S0277-3791(03)00081-7, 2003.

Radić, V. and Hock, R.: Regionally differentiated contribution of mountain glaciers and ice caps to future sea-level rise, Nat. Geosci., 4, 91–94, doi:10.1038/ngeo1052, 2011.

Roe, P. L.: Characteristic-based schemes for the Euler equations, Annu. Rev. Fluid Mech., 18, 337–365, doi:10.1146/annurev.fluid.18.1.337, 1986.

van Leer, B.: Towards the ultimate conservative difference scheme. V. A second-order sequel to Godunov's method, J. Comput. Phys., 32, 101–136, doi:10.1016/0021-9991(79)90145-1, 1979.

TCD
6, 4037–4069, 2012

Mountain glacier model benchmark

A. H. Jarosch et al.

Table 1. Relative volume errors, $RE_{vol} = (V_{numerical} - V_{exact})/V_{exact} \cdot 100$, for our schemes and the type I scheme for different spatial resolutions. $V_{exact} = 4.443984 \times 10^6\,m^2$ in the 2-D case described in Sect. 7 with results plotted in Fig. 3.

Δx	RE_{vol} MUSCL minmod	RE_{vol} MUSCL superbee	RE_{vol} type I
1000 m	−8.024 %	−5.605 %	121.568 %
500 m	−4.419 %	−3.038 %	137.077 %
250 m	−2.088 %	−1.328 %	144.522 %
200 m	−1.622 %	−1.012 %	146.000 %
125 m	−0.892 %	−0.488 %	148.213 %

TCD
6, 4037–4069, 2012

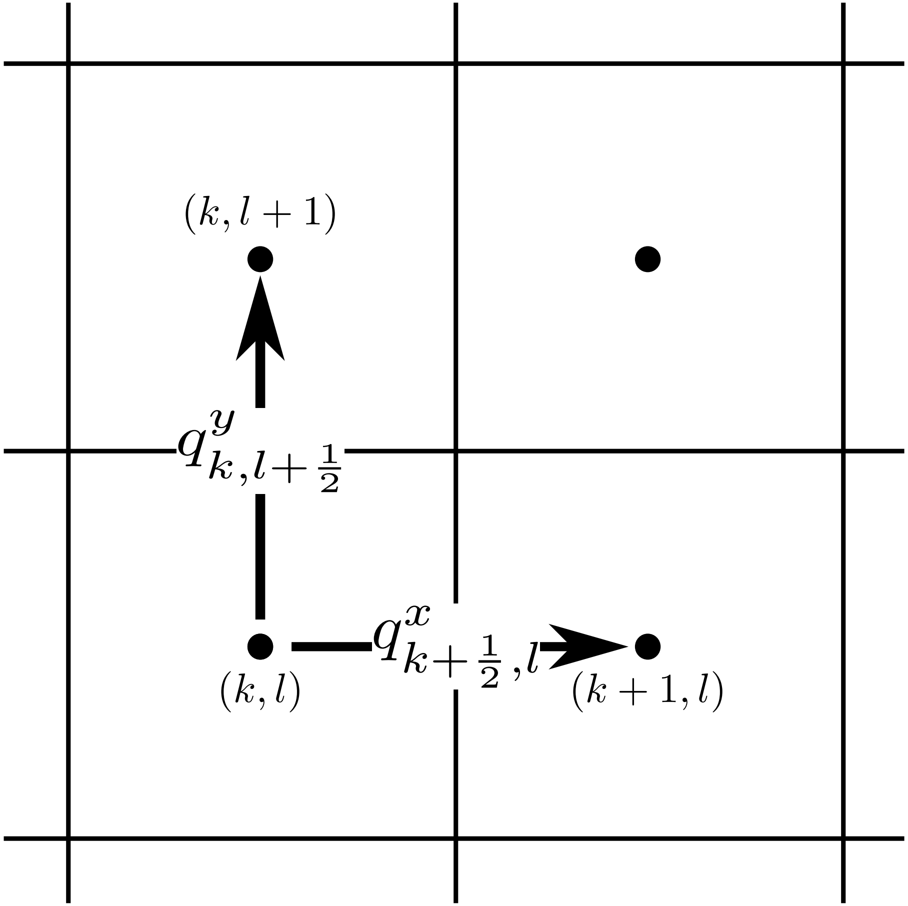

Fig. 1. Basic grid setup and definition of fluxes.

TCD
6, 4037–4069, 2012

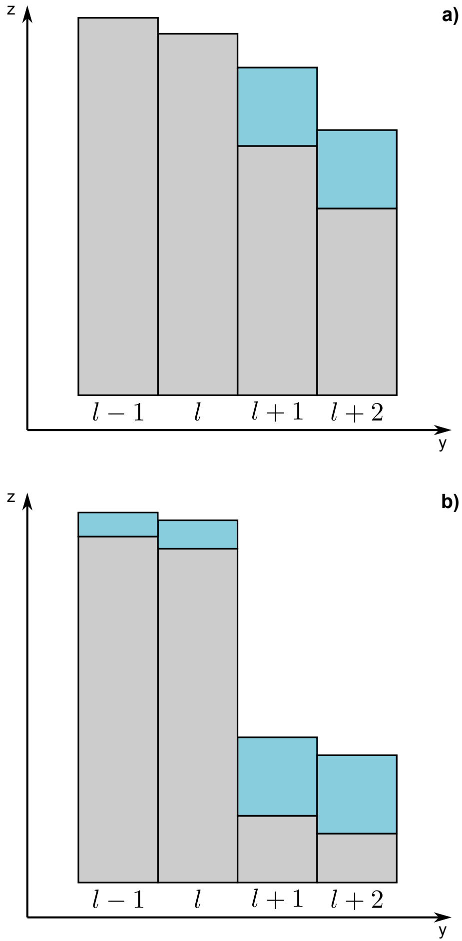

Fig. 2. The valley glacier case in **(a)** and the icefall case in **(b)**. Bedrock in grey and ice in light blue.

TCD
6, 4037–4069, 2012

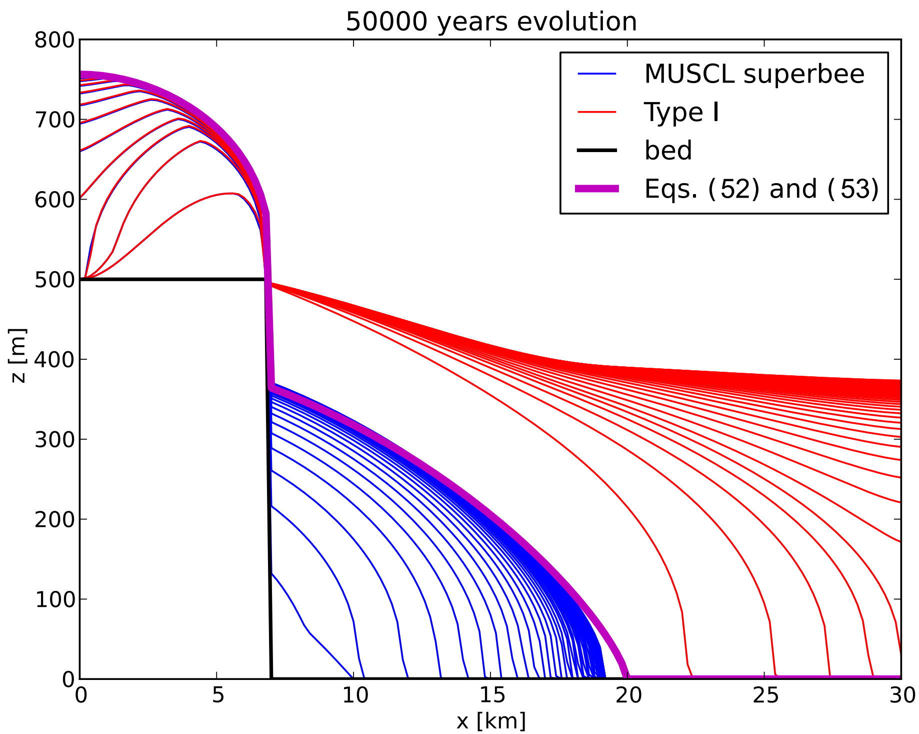

Fig. 3. Comparison of the "MUSCL superbee" scheme (blue lines) with a classical "type I" scheme (red lines) and a solution computed with Eqs. (52) and (53) (magenta line). For both numerical schemes, solutions are plotted at 1000 yr intervals for a 50 000 yr evolution.

TCD
6, 4037–4069, 2012

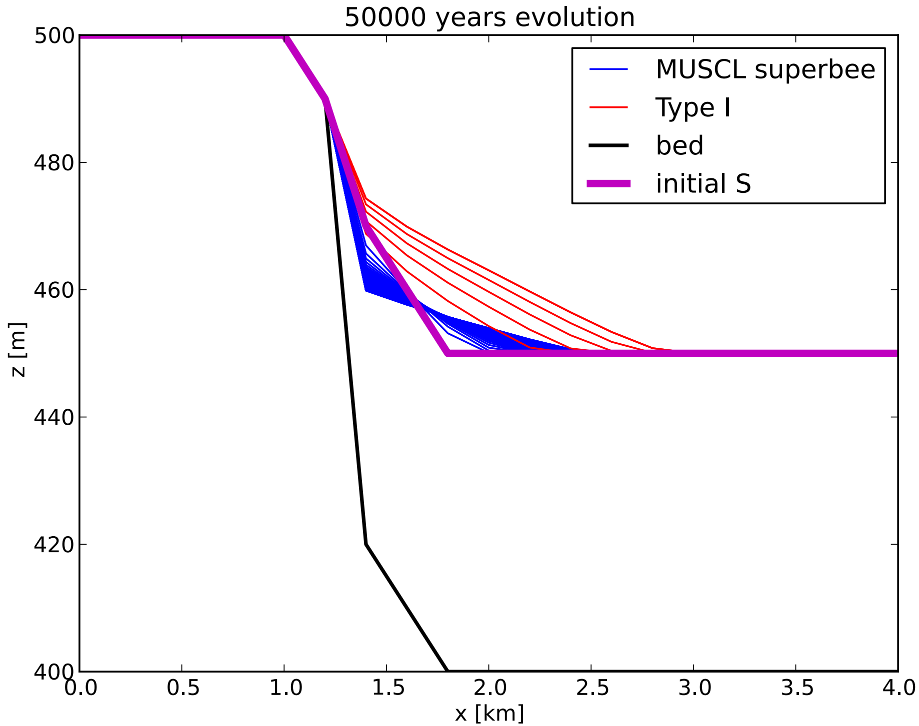

Fig. 4. Comparison of the "MUSCL superbee" (blue lines), with a classical "type I" scheme (red lines) for the mass conservation problem described in Sect. 3. The initial surface is displayed as a magenta line. For both numerical schemes, solutions are plotted at 1000 yr intervals for a 50 000 yr evolution.

TCD
6, 4037–4069, 2012

Mountain glacier model benchmark

A. H. Jarosch et al.

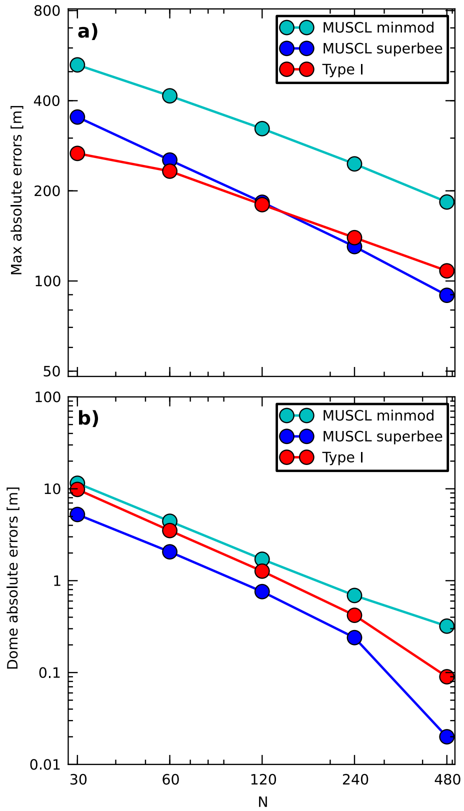

Fig. 5. Results of the Bueler C benchmark (cf. Sect. 7.2) for increasing grid point number N on a log-log scale. The maximum error in the whole domain, e_{max}, is displayed in **(a)**, and **(b)** shows the central dome height error e_{dome}.